ANTIOXIDANTS & REDOX SIGNALING
Volume 12, Number 8, 2010

DOI: 10.1089/ars.2009.2917

ORIGINAL RESEARCH COMMUNICATION

Nox-4–Dependent Nuclear H_2O_2 Drives DNA Oxidation Resulting in 8-OHdG as Urinary Biomarker and Hemangioendothelioma Formation

Gayle Gordillo,[1,2] Huiqing Fang,[1] Hana Park,[2] and Sashwati Roy[2]

Abstract

Hemangioendotheliomas are classified as endothelial cell tumors, which are the most common soft tissue tumors in infants. In a murine model of hemangioendothelioma, we previously showed that MCP-1 is required for its development and that the expression of MCP-1 in EOMA cells is redox sensitive. Here, we sought to identify the source of oxidants that drive hemangioendothelioma formation. Seven known isoforms exist of the catalytic subunit gp91. Only the nox-4 isoform of gp91 was present in EOMA cells, in contrast with non–tumor-forming murine endothelial cells that contained multiple forms of nox. Nox-4 knockdown markedly attenuated MCP-1 expression and hemangioendothelioma formation. We report that in EOMA cells, nox-4 is localized such that it delivers H_2O_2 to the nuclear compartment. Such delivery of H_2O_2 causes oxidative modification of DNA, which can be detected in the urine of tumor-bearing mice as 8-hydroxy-2-deoxyguanosine. Iron chelation by *in vivo* administration of deferoxamine improved tumor outcomes. The current state of information connects nox-4 to MCP-1 to form a major axis of control that regulates the fate of hemangioendothelioma development *in vivo*. *Antioxid. Redox Signal.* 12, 933–943.

Introduction

HEMANGIOMAS are the most common soft tissue tumor in infants, affecting 3 to 10% of all infants (16, 35, 37). Hemangiomas are a clonal proliferation of a transformed endothelial cell and are classified as endothelial cell tumors (8). The classification of endothelial cell tumors also includes hemangioendotheliomas, which are much rarer, but the pharmacologic regimens for treating both hemangiomas and hemangioendotheliomas are exactly the same. Like many other solid tumors, endothelial cell tumors express monocyte chemoattractant protein-1 (MCP-1) (25). The extent of macrophage infiltration in solid tumors generally correlates directly with tumor progression, as macrophages are obligate partners in making possible angiogenesis, malignant cell migration, invasion, and metastases (10, 40). These conclusions are based not only on correlations observed in clinical studies, but also on experimental evidence that shows that ablation of macrophage function or infiltration into experimental tumors inhibits growth and metastases (20, 31, 32). By using a validated murine endothelial (EOMA) cell tumor model, we previously demonstrated that MCP-1 protein expression in EOMA cells is redox sensitive, that MCP-1 expression is required for endothelial cell (EC) tumor formation, and that antioxidant treatments directed at inhibiting MCP-1 expression in EOMA cells can decrease EC tumor incidence, size, and mortality (2, 19–21). In this work, we sought to identify the source of oxidants stimulating MCP-1 expression in EOMA cells because understanding the signaling mechanisms that result in MCP-1 expression will provide greater insight into the underlying pathologic processes that make EC tumor formation possible.

Materials and Methods

Cell culture

Murine aortic endothelial (MAE) cells were maintained under the same conditions as EOMA cells, as previously described (19–21). In brief, EOMA cells (www.atcc.org) are maintained in DMEM supplemented with 10% fetal calf serum (FCS) and 1% penicillin/streptomycin, also referred to as normal growth medium (NGM), and incubated at 37°C and 5% CO_2. siRNA sequences were obtained from Dharmacon for either nox-4 or control/scrambled siRNA. Transfections were performed by using ON-TARGET plus and SMART pool technologies (Dharmacon) in which four different sets of

[1]Division of Plastic Surgery, and [2]Laboratory of Molecular Medicine, Department of Surgery, Davis Heart Lung Research Institute, The Ohio State University, Columbus, Ohio.

nox-4 siRNA sequences are pooled together for transfection to increase specificity. EOMA cells were transiently transfected by using DharmaFECT 1, according to the manufacturer's protocol (Dharmacon, Lafayette, CO). EOMA cells were stably transfected with 58-bp lentiviral shRNA particles (Sigma, St. Louis, MO) for either nox-4 shRNA: (5′-CCGGGCATT AGTCTTAACCAGACATCTCGAGATGTCTGGTTAAGACT AATGCTTTTTG-3′) or control/scrambled shRNA. EOMA cells EOMA cells (7×10^4 cells/well) were seeded in 12 well plates with 1 ml of media containing 8 μg/ml of hexadimethrine bromide (Sigma). Lentiviral particles were added at 2, 10, or 50 multiplicity of infection (MOI) into 110 μl of media containing 8 μg/ml of hexadimethrine bromide. Media was changed every 24 h by using NGM for the next 5 days. At 48 h, puromycin was added at 2.0 μg/ml, and at day 5 after transfection, surviving clones were isolated and maintained in NGM + 2 μg/ml puromycin. Effective knockdown of nox-4 with either form of RNA interference was confirmed by real-time PCR and Western blot.

In vivo *studies*

Mice were fed standard chow and water *ad libitum* and housed in clean environments in compliance with Institutional Laboratory Animal Care and Use Committee guidelines. Female 129P/3 mice (Jackson Laboratories, Bar Harbor, ME) between 6 and 8 weeks of age and weighing 15 to 20 grams received subcutaneous injection of EOMA cells, as previously described (21). Subcutaneous injection of EOMA cells results in formation of an EC tumor histologically classified as a kaposiform hemangioendothelioma (KHE). Serum samples were obtained by retroorbital bleed before EOMA cell injection to determine baseline oxidative measurements. Urine specimens were collected by placing mice in sterile cages containing water bottles, but no bedding. Urine was collected from the bottom of the cage every 2 h over the course of an 8-h day by aspirating isolated pools of urine on the bottom of the cage that were free of contamination with feces or other debris. Urine samples were spun at 2,500 $g\times10$ min and stored at -80°C until ready for use. Tumor volume was determined by using calipers to measure length×width×height of each tumor, and the mass was determined by draining the blood from the tumor and weighing the residual solid tumor mass dissected free from any surrounding soft tissue.

Single-cell microinjection

EOMA cells (1.5×10^5/plate) were grown in NGM on 35-mm plates 24 h before microinjection. Microinjection was performed by using a micromanipulator Femtojet B 5247 and Injectman NI 2 (Eppendorf, Hamburg, Germany) with 80 hectopascal (hPA) of pressure and 0.2-s duration. The compensation pressure during injection was 40 hPa. The glass micropipettes were made from GD-1 glass capillaries (Narishige, Tokyo, Japan) by using a Narishige PC-10 Puller with heater set at 52.7°C. Catalase (0.1 milliunits/cell) was microinjected into either cytoplasm or nucleus of EOMA cells and then immediately injected with DCF(125 attomoles/cell). All DCF was delivered by cytoplasmic injection. Catalase (Sigma) was co-injected with QDot streptavidin conjugate (Invitrogen, Carlsbad, CA) with the emission maximum near 605 nm. QDot streptavidin conjugate was used as a fluorescent marker to localize the injection site. Digital images were collected by using a specialized phase contrast as well as a fluorescent Zeiss Axiovert 200M microscope suited for imaging cells grown in routine culture plates. The sample stage was maintained at 37°C, and the sample gas environment was maintained exactly as in the culture incubator. Fluorescence densitometry was calculated by using AxioVision LE software version 3.1 (www.zeiss.com).

Western blot

Immunoblotting was performed by using EOMA cell lysates with 50 μg protein/nox-4 sample and 10 μg protein/beta-actin sample transferred to nitrocellulose membranes. A rabbit polyclonal anti-nox-4 antibody (Novus Biologicals, Littleton, CO) was used at a 1:500 dilution. Bands were visualized by using horseradish peroxidase–conjugated anti-rabbit IgG (Amersham Biosciences) at 1:2,000 dilution and the enhanced chemiluminescence assay (Amersham Biosciences, Piscataway, NJ), according to the manufacturer's instructions.

Flow-cytometry detection of oxidants

Cells were seeded in 12-well plates at 10^5 cells/well, incubated overnight, and collected by trypsinization with each individual well resuspended in 200 μl PBS and tubes placed on ice. For detection of DCF oxidation, a 200-μl aliquot of 40 μM 5-(and-6)-carboxy-2′,7′ dichlorofluorescein–diacetate (DCF) (Invitrogen) in PBS was added to each tube, mixed by pipetting, incubated in a 37°C water bath, and placed on ice and protected from light. DCF oxidation was detected by using an Accuri C6 Flow Cytometer (Accuri, Ann Arbor, MI) on the FL1 channel (530-nm emission detection) setting with a gated sample size of 10,000 cells. For detection of superoxide production in cells, the same protocol was used, except that cells were incubated with 10 μM dihydroethidium (DHE) (Invitrogen), and the flow-cytometer settings were channel FL2 (585-nm emission detection).

Nox-4 immunolocalization

EOMA cells (4×10^4 cells/well) were placed on a 12-mm glass coverslip (Fisher) placed in a 12-well culture dish, covered with NGM, and incubated for 24 h. Cells were permeabilized by adding 0.1% Triton X-100 in PBS and then washed thrice with PBS. The cells were then incubated with 10% bovine serum albumin in PBS for 1 h at room temperature. The primary antibody used was a rabbit polyclonal anti-nox-4 antibody (Novus Biologicals), and it was added at 1:70 dilution in PBS. Cells were washed thrice with PBS and the secondary antibody Alexa Fluor green 488 goat anti-rabbit IgG (Invitrogen) added at 1:500 dilution and incubated at room temperature for 45 min. The nucleus was then counterstained by adding 1:10,000 dilution of DAPI (Invitrogen) to each well and incubated for 2 min. The coverslips were placed on glass microscope slides with fluorescence mounting medium (Vector Laboratories), and images were obtained with green and blue filters on a Zeiss 200M Axiovert microscope at 200× magnification.

mRNA quantification

Total RNA was isolated from cells by using the Absolutely RNA Miniprep kit (Stratagene). mRNA was reversed transcribed to cDNA by using SuperScript III First-Strand

Synthesis System for RT-PCR (Invitrogen). The abundance of mRNA for genes of interest was quantified by using real-time polymerase chain reaction (PCR) with double-stranded DNA-binding dye SYBR green-I. The following primer sets (Invitrogen) were used:

m_JE/MCP-1 F: 5′-GAA GCT GTA GTT TTT GTC ACC AAG C-3′; ***m_JE/MCP-1 R:*** 5′-GAT CTC ATT TGG TTC CGA TCC AG-3′; ***m_GAPDH F***: 5′-GGT CAC CAG GGC TGC CAT TT-3′; ***R*** 5′-GGG CTT CCC GTT GAT GAC AAG-3′; ***m_nox-1 F***: 5′-CAC CCC CCT GAG TCT TGG AA-3′; ***m_nox-1 R***: 5′-GGG TGC ATG ACA ACC TTG GTA ATC-3′; ***m_nox-2 F***: 5′-GGA ATT GTC ATC ACA CTG TGT CTC A-3′; ***m_nox-2 R***: 5′-GTA CAA TTC GTT CAG CTC CAT GG-3′; ***m_nox-3 F***: 5′-ACA CGG ATG AGT GAA CAA GGG AAG-3′; ***m_nox-3 R***: 5′-ATC CAC AGA AGA ACA CGC CAA TGC-3′; ***m_nox-4 F***: 5′-CAC CTC TGC CTG CTC ATT TGG-3′; ***m_nox-4 R***: 5′-AGT TGA GGT TCA GGA CAG ATG CA-3′; ***m_duox 1 F***: 5′-TTC CAG AAG GTG CTG AAC AGG AGT-3′; ***m_duox 1 R***: 5′-TGA GCT GAC AAG CCT TCT CCA CAT-3′; ***m_duox 2 F***: 5′-AAC CAC CTA TGT GGG CAT CAT CCT-3′; ***m_duox 2 R***: 5′-AGG ACA ACT GCA GCC ATA GCA ATC-3′.

Hydrogen peroxide assay

Amplex red assay was performed according to the manufacturer's instructions (Invitrogen). In brief, cells were grown in 12-well plates at 1×10^5 cells/well in phenol red–free DMEM + 10% FCS and 1% pen/strep. Cells were incubated for 24 h, and then Amplex red assay was performed. Spectrophotometric readings were obtained at 530-nm excitation and 590-nm fluorescence detection by using a Bio-TEK ELX 808IU microplate reader (Bio-TEK Instruments).

Detection of 8-OHdG

Urine samples were thawed on ice, and an 8-OHdG ELISA-based assay was performed according to the manufacturer's instructions (BioVendor). In brief, 40 μl of urine was added to 120 μl of antibody diluent, and a 50-μl aliquot of this solution plus 50 μl of primary antibody solution was added to a 96-well plate. The plate was sealed and incubated at 4°C overnight. Next, the plate was washed thrice, and 100 μl of secondary antibody was added and incubated for 1 h at room temperature. The plate was washed thrice and incubated with 100 μl of horseradish peroxidase solution for 15 min before a stop solution was added. Spectrophotometric readings were obtained at OD 450 nm by using a Bio-TEK ELX 808IU microplate reader (Bio-TEK Instruments).

Cell-cycle analysis

Cell cycles were synchronized by serum starving with DMEM + 0.5% FCS + 1% pen/strep for 48 h before performing cell-cycle analysis with propidium iodide (26) by using CellQuest software (BD Biosciences).

MCP-1 ELISA

EOMA cells were seeded in 12-well plates at 8×10^4 cells/well. MCP-1 ELISA was performed on cell supernatants by using the CCL2/JE/MCP-1 Quantikine ELISA kit (R&D Systems, Minneapolis, MN) according to the manufacturer's instructions. Absorbance was detected at 450 nm. Bio-Rad protein assay was performed on an aliquot of all tested samples and the results standardized per milligram of protein.

BrdU assay

EOMA cells in 100 μl NGM were seeded in flat-bottom 96-well culture plates at 3,000 cells/well and incubated overnight. ELISA-based BrdU assay was performed according to the manufacturer's instructions (Roche, Indianapolis, IN). Once the colorimetric substrate was added, incubation was kept to <5 min, and absorbance was read at 450 nm by using a Bio-TEK ELX 808IU microplate reader.

Matrigel angiogenesis assay

EOMA cells were trypsinized, resuspended in media at 6×10^4 cells/ml, and 500 μl of cell suspension was seeded on growth factor–reduced, phenol red–free Matrigel (BD Biosciences, Bedford, MA), prepared according to the manufacturer's instructions in four-well tissue-culture plates (Nunc, Rochester, NY). The cells placed on Matrigel were incubated at 37°C and 5% CO_2 overnight. Cell cytoplasms were fluorescently stained by adding 0.5 μl of Calcein AM (Invitrogen) (8.3 μg/μl DMSO) to each well and incubating at 37°C and 5% CO_2 for 15 to 60 min. Fluorescent images were obtained immediately by using a Zeiss Axiovert 200M microscope. Tube formation was quantified by examining three images per well by using AxioVision LE software version 3.1 (www.zeiss.com) to measure total area within the tubes for a standard 50× magnification image.

Statistical methods

Data for all figures are presented as the mean ± standard deviation. For all figures, except Fig. 10a, two-tailed t tests were performed (Microsoft Excel). Figure 10a required comparisons between multiple groups, so analysis of variance (ANOVA) was performed. When F values were significant, a *post hoc* analysis by using a Kruskal–Wallace test was also performed. All calculations were performed by using SPSS software (SPSS, Chicago, IL) A p value <0.05 was considered significant.

Results

Oxidative stress is widely accepted as contributing to the neoplastic transformation process. We sought to determine whether excess oxidant production was present in EOMA cells. We compared the incidence of oxidant load in EOMA cells *versus* MAE cells. MAE cells were selected because they are murine endothelial cells that are transformed with regard to their ability to propagate in culture, just like EOMA cells. However, EOMA cells but not MAE cells can make a tumor when injected subcutaneously into mice. DCF is a nonspecific indicator of oxidant load in cells. Flow-cytometry results indicated that DCF oxidation was significantly greater in EOMA cells compared with results from MAE cells (Fig. 1a). The major source of reactive oxygen species (ROS) in ECs is NADPH oxidase (3, 18). The reaction catalyzed by NADPH oxidase is the reduction of molecular oxygen to superoxide (O_2^-), which is a highly unstable product that can dismutate into hydrogen peroxide (H_2O_2) either enzymatically or spontaneously. Flow cytometry was used to measure the oxidation of DHE, which occurs specifically in response to superoxide production (28, 38). Although EOMA cells showed more DCF oxidation, when tested with DHE, these cells showed lower DHE oxidation, indicating lower levels of

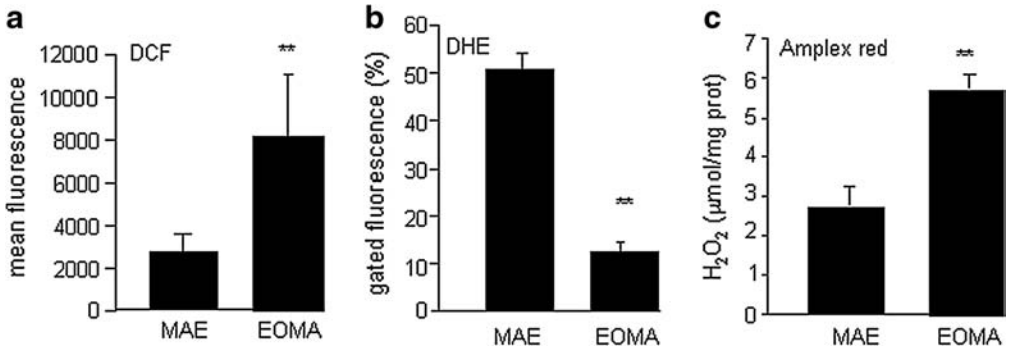

FIG. 1. H_2O_2, not the superoxide form of ROS, is abundant in EOMA cells. (**a**) EOMA cells and non–tumor-forming murine aortic endothelial (MAE) cells were treated with 5-(and-6)-carboxy-2′,7′ dichlorofluorescein diacetate (DCF), and oxidation was detected with flow cytometry. (**b**) Dihydroethidium (DHE) specifically detects superoxide production with red fluorescence (570 nm). Low DHE oxidation in EOMA cells indicates that the contribution of superoxide to DCF oxidation is low. (**c**) Amplex red assay (Invitrogen) showed that H_2O_2 levels were significantly elevated in EOMA cells compared with nontumor MAE cells. $^{**}p < 0.01$.

superoxide compared with MAE (Fig. 1b). These observations also suggest that the DCF oxidation signal noted in EOMA cells was not contributed by superoxide anion radicals. Indeed, quantitative measurements of H_2O_2 by using the Amplex red assay showed that H_2O_2 accounted for a large fraction of the DCF oxidation signal (Fig. 1c).

To investigate the source of ROS produced by these cells, we sought to determine the abundance of NADPH oxidase enzyme components in each cell type. Real-time PCR was used to screen for the six known isoforms of gp91 present in rodents and to determine which ones were present in these cells. Strikingly, only the nox-4 isoform was detectable in EOMA cells (see Fig. 2a). In contrast, the non–tumor-forming MAE cells had multiple forms of nox in appreciable abundance (Fig. 2b). This observation on MAE cells is consistent with previously published reports of gp91 isoforms present in ECs.

Quantitative PCR results showed that EOMA cells contain nox-4 mRNA levels 68 times greater than those present in MAE cells (Fig. 2c). These results support the findings reported in Fig. 1 because nox-4 is unique among the gp91 isoforms. It is the only isoform of gp91 that is constitutively active, and the only bioavailable form of ROS generated as a result of its activity is H_2O_2 and not superoxide (5, 14). Thus, the gp91 profile explains the lack of superoxide activity in EOMA cells.

An RNA interference approach was used to test whether nox-4 indeed regulates H_2O_2 production in EOMA cells. EOMA cells subjected to nox-4 knockdown showed 50% attenuation in DCF oxidation, suggesting that nox-4 is a significant contributor to DCF-sensitive oxidants in EOMA cells (Fig. 3a). Results from the Amplex red assay demonstrated that in EOMA cells, nox-4 is a significant contributor to H_2O_2 production (Fig. 3b). To examine the significance of nox-4 in EOMA cells, stable transfectants were generated by using nonreplicating lentiviral particles designed as either nox-4 shRNA or control shRNA. This approach effectively downregulated both nox-4 gene and protein (Fig. 4a and b) and reduced H_2O_2 production (Fig. 3b).

Hydrogen peroxide is known to stimulate angiogenesis and cell proliferation, two fundamental events in tumor development. Our observation that EOMA cells possess only the nox-4 isoform of gp91 led to the hypothesis that it may play a central role in EC tumor development. To test this hypothesis, we injected 129P/3 mice with EOMA cells stably transfected with either control shRNA or nox-4 shRNA. It should be

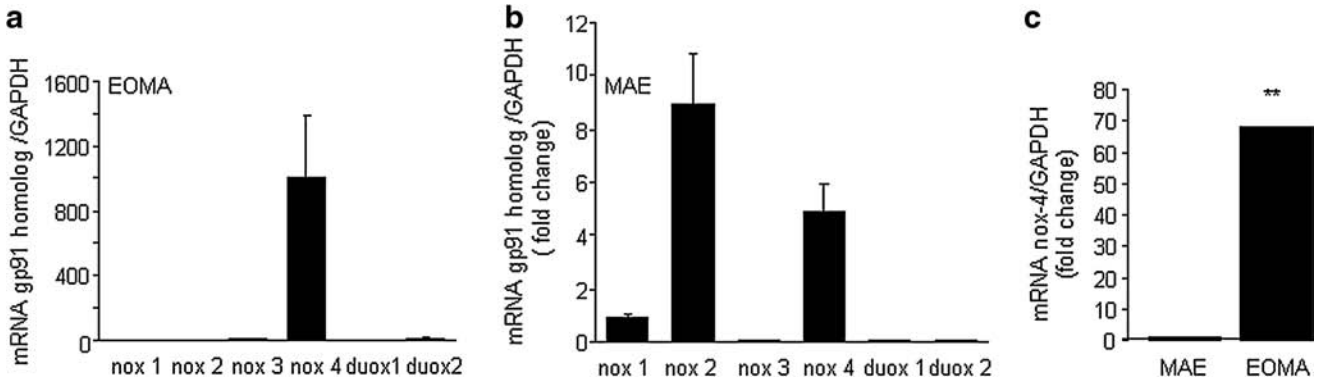

FIG. 2. Nox-4 is the predominant homologue of gp91present in EOMA cells. Real-time PCR was done on mRNA from (**a**) tumor-forming EOMA cells or (**b**) non–tumor-forming murine aortic endothelial (MAE) cells. Both cells lines are transformed murine endothelial cell lines that grow readily in culture, but only the EOMA cells make tumors when injected into mice. (**c**) The abundance of nox-4 mRNA is 68-fold higher in EOMA compared with MAE cells. Error bars are too small to be visible. $^{**}p < 0.01$.

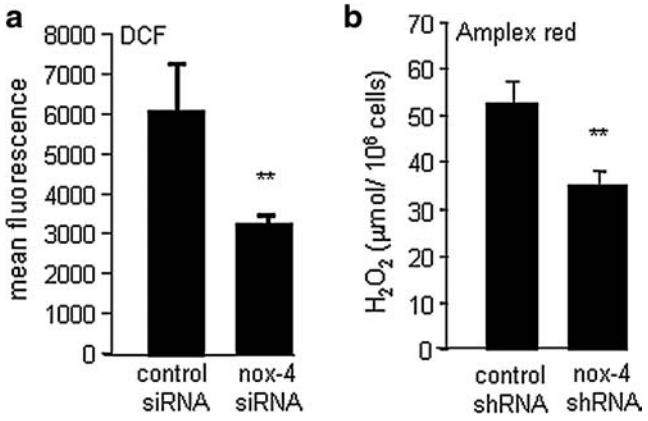

FIG. 3. Nox-4 contributes to H_2O_2 levels in EOMA cells. (**a**) Knockdown of nox-4 activity resulted in a significant decrease in DCF oxidation. (**b**) H_2O_2 levels as determined by Amplex red assay. Knockdown of nox-4 significantly decreased H_2O_2 levels. $^{**}p < 0.01$.

noted that EOMA cells are derived from a spontaneously arising kaposiform hemangioendothelioma (KHE) in 129 P/3 mice, so they are syngeneic with this strain, enabling these tumors to be studied in the context of a completely functional immune system. Mice injected with EOMA cells develop KHE with 100% efficiency. As result of KHE formation, the mice sequester platelets and red blood cells within the tumor itself, resulting in anemia, high-output heart failure, and death (a process that also can occur in humans with KHE) beginning ~7 days after EOMA cell injection. KHE specimens were harvested 7 days after EOMA cell injections. The mice that received the nox-4 knockdown EOMA cells demonstrated significantly smaller KHE compared with those that received EOMA cells transduced with control shRNA (Fig. 4c).

The finding that nox-4 plays a significant role in stimulating EC tumor development then led to a series of experiments to determine the mechanisms mediating the effects of nox-4. We previously showed the MCP-1 is required for EC tumor formation (20). MCP-1 may represent the final common end point of an underlying series of signaling events that lead to EC tumor formation. An siRNA approach was used to determine whether nox-4 stimulates MCP-1 expression in EOMA cells. Knockdown of nox-4 activity in EOMA cells was confirmed by using real-time PCR and Western blot (Fig. 5a and b). Knockdown of nox-4 resulted in a statistically significant decrease in MCP-1 gene as well as protein expression (Fig. 5c and d).

Next, the significance of nox-4 to stimulate angiogenic responses in EOMA cells was investigated. Angiogenic capacity is required for solid-tumor growth of any kind, but in EC tumors, it uniquely represents the growth capacity of the tumor itself. Injected EOMA cells establish a connection with the host vasculature to become blood-filled/perfused tumors. These lesions do not metastasize but have aggressive local growth through progressive unregulated angiogenesis. Knockdown of nox-4 resulted in a dramatic decrease in the angiogenic properties of EOMA cells in Matrigel (Fig. 6a and b). This response was objectively scored by measuring the area within enclosed angiogenic rings (Fig. 6c).

Dysregulated cell proliferation is a hallmark of tumor formation, and NADPH oxidase has been shown to regulate EC proliferation (9). To investigate whether nox-4 influenced cell-cycle regulation, a BrdU assay was performed on EOMA cells transduced with lentiviral shRNA particles containing either control shRNA or nox-4 shRNA. Knockdown of nox-4 resulted in a significant decrease in EOMA cell proliferation (Fig. 7a). More precisely to determine where nox-4 influences the progression through the cell cycle, flow-cytometry studies were conducted by using propidium iodide. When nox-4 expression was downregulated, cells accumulated at the G_2-M transition (Fig. 7b), suggesting that nox-4 allows cells to bypass the post-replicative checkpoint that prevents damaged DNA from being duplicated. Thus, results from cell-cycle analyses suggested that nox-4 may contribute to DNA damage, another hallmark of the neoplastic transformation process. If nox-4 is localized in the nuclear membrane, it would suggest that the ROS produced as a result of its activity would be localized in the nuclear/perinuclear compartment. Such distribution of ROS would have DNA within striking

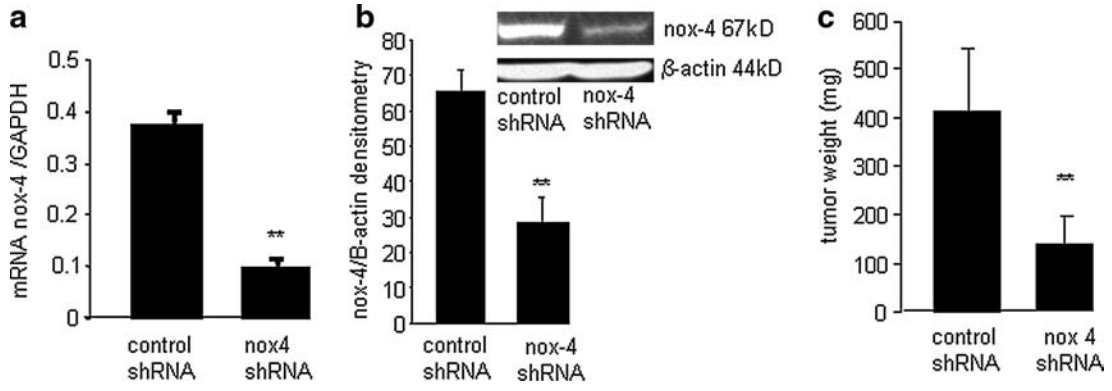

FIG. 4. Nox-4 knockdown arrested kaposiform hemangioendothelioma growth *in vivo*. EOMA cells were transduced with a nonreplicating lentiviral vector containing shRNA for either nox-4 or a nontargeting negative control (scramble) sequence. Puromycin selection was performed to select the clone with the most efficient knockdown of nox-4, as determined by (**a**) real-time PCR and (**b**) Western blot. Significant knockdown of nox-4 gene and protein was achieved. $^{**}p < 0.01$. (**c**) EOMA cells stably transfected with nox-4 or control/scrambled shRNA were injected subcutaneously into 129P/3 mice. Tumors were harvested at 7 days after EOMA cell injection. Mice injected with EOMA cells transduced with nox-4 shRNA had significantly smaller tumors compared with those receiving EOMA cells with control shRNA. $^{**}p < 0.01$.

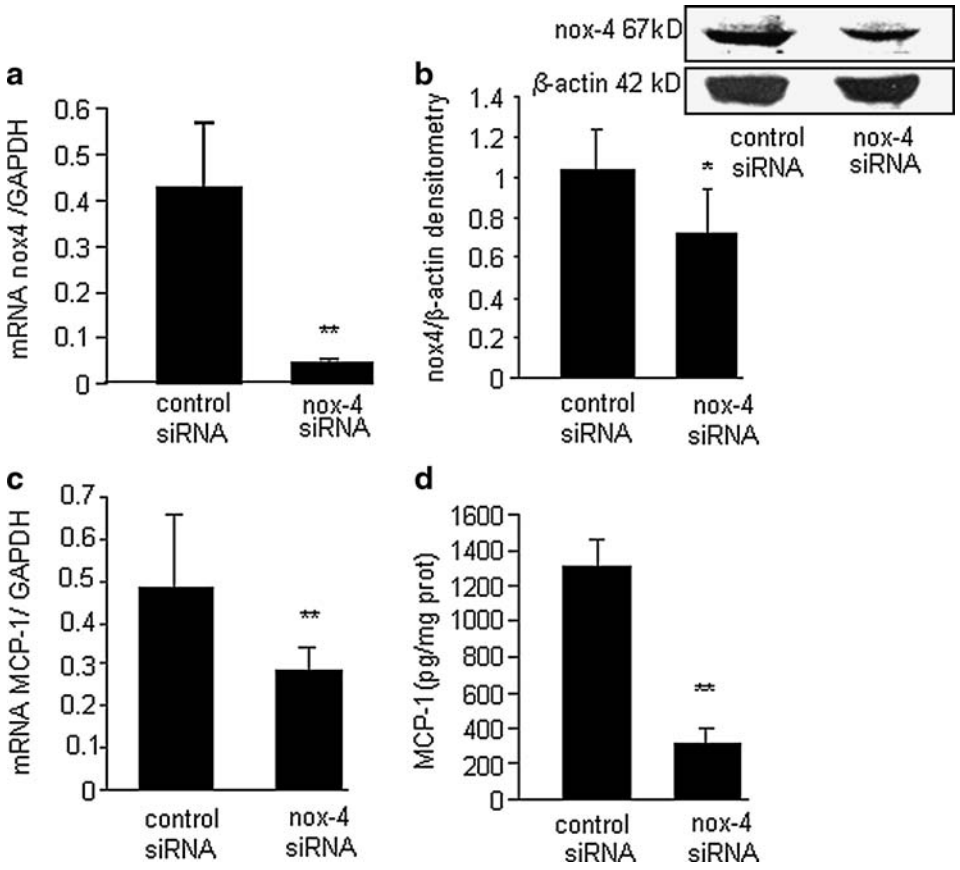

FIG. 5. MCP-1 expression in EOMA cells is nox-4 dependent. (**a**) Real-time PCR confirmed knockdown of the nox-4 gene. (**b**) Western blot demonstrates decreased levels of nox-4 protein in knockdown cells. (**c**) Real-time PCR for MCP-1 mRNA shows that knockdown of nox-4 attenuates MCP-1 gene expression. (**d**) ELISA for MCP-1 protein shows that knockdown of nox-4 attenuates MCP-1 protein expression. $^{**}p < 0.01$.

distance, causing oxidative modification of DNA. Immunofluorescence studies revealed localization of nox-4 in the nuclear membrane (Fig. 8a). Knockdown of nox-4 attenuated the immunofluorescence signal, demonstrating specificity of the antibody used for nox-4. To obtain direct evidence on H_2O_2 localization in EOMA cells, DCF was microinjected into single cells. DCF oxidation was highly prominent in the nuclear compartment. Such a nuclear DCF oxidation signal was eliminated by microinjection of catalase in the nucleus, demonstrating that the nucleus of EOMA cells is loaded with high levels of H_2O_2 (Fig. 9). In this study, catalase was co-injected with streptavidin-based Qdot label to verify the location of the injection. This experiment was repeated by using catalase without the Qdot to demonstrate that the lack of DCF fluorescence was not due to masking from the red fluorescent streptavidin (see Supplemental Fig. 1; www.liebertonline.com/ars). Taken together, these results indicate that nox-4 is localized to the nuclear membrane in tumor-forming EOMA cells and that the H_2O_2 generated as a result of nox-4 activity is abundant in the nuclear compartment.

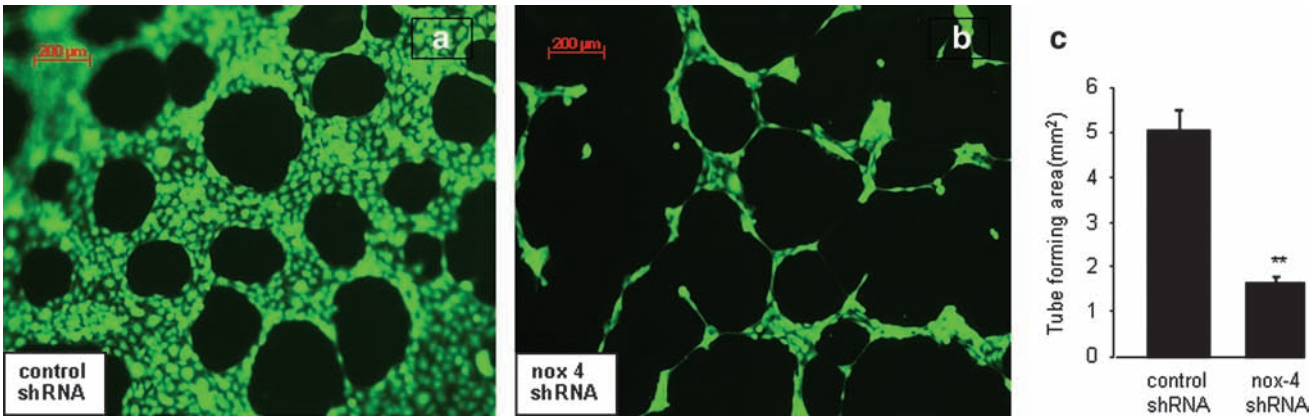

FIG. 6. Nox-4 knockdown disrupts angiogenic tube formation of EOMA cells. To determine the contribution of nox-4 to the angiogenic property of EOMA cells, an *in vitro* assay was performed by using EOMA cells transduced with either (**a**) control shRNA or (**b**) nox-4 shRNA and seeded on reduced growth factor Matrigel. Cells were stained with calcein-AM, and the area within the formed tubes was quantitated by using AxioVision LE software. (**c**) Tube formation by EOMA cells was significantly blunted in response to nox-4 knockdown. $^{**}p < 0.01$. (For interpretation of the references to color in this figure legend, the reader is referred to the web version of this article at www.liebertonline.com/ars).

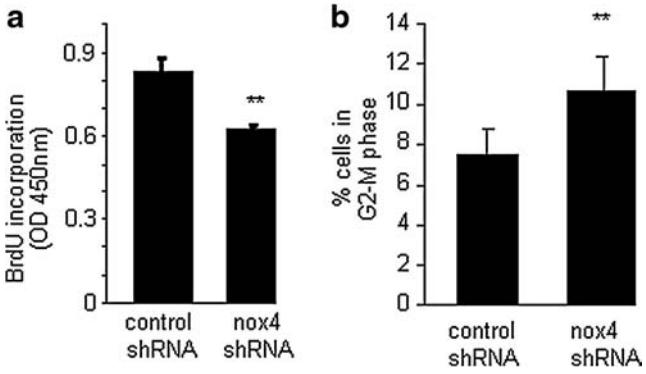

FIG. 7. Nox-4 contributes to EOMA cell proliferation and progression through the G_2-M cell-cycle checkpoint. (**a**) BrdU assay showed a significant attenuated proliferation of nox-4 knockdown cells. (**b**) Nox-4 knockdown caused cells to accumulate in the G_2-M transition phase of the cell cycle. $^{**}p < 0.01$.

Finally, to determine whether the finding of nox-4 localization to the nuclear membrane is biologically significant, we measured the levels of oxidatively modified DNA in the urine of mice with KHE by using an 8-hydroxy-2′-deoxyguanosine (8-OHdG) ELISA kit. Pooled urine specimens were collected from 129 P/3 mice at multiple points before and after EOMA cell injection. Compared with baseline levels, a significant increase was found in the amount of oxidized DNA excreted in the urine, correlating with tumor progression (Fig. 10a). For nox-4 activity to result in DNA oxidation, the H_2O_2 produced would have to be converted to hydroxyl radicals. We postulated that this would occur through Fe^{2+}, which is abundant in the nucleus. To test this hypothesis, mice injected with EOMA cells were treated with deferoxamine (DFO), an iron chelator. Mice that received a daily dose of DFO (100 mg/kg), given by intraperitoneal (IP) injection, had significantly smaller tumors compared with mice receiving an IP injection of PBS (100 μl) vehicle control (Fig. 10b and c).

Discussion

NADPH oxidases represent an enzyme system now implicated in the etiology of a wide range of diseases (1, 4, 7, 12, 15, 17, 22, 23, 30, 33, 34, 39, 42, 47, 49). NADPH oxidases represent the major source of ROS production in ECs (1, 4, 17, 23, 39). Seven homologues of gp91 exist: nox-1, nox-2, nox-3, nox-4, nox-5, duox1, and duox 2. Nox-5 is absent in rodents (27), and nox-1, nox-2, nox-4, and nox-5 are reported to be found in human ECs (18). This work recognizes nox-4 as the primary form of the gp91 catalytic subunit of NADPH oxidase that is abundant in EOMA cells. Compared with non–tumor-forming cells such as MAE, the presence of nox-4 as the sole NADPH oxidase enzyme is unique to EOMA cells. The fact that EOMA cells express only nox-4 and that it deviates from other reported profiles of endothelial cells as possessing some combination of nox-1, nox-2, and nox-4 leads to the speculation that change in the gp91 expression profile occurs as a result of the tumor-initiation process. For example, recent reports linking mutations in the gene for isocitrate dehydrogenase (IDH) with glioblastoma formation may represent such an initiating event, because IDH regulates NADPH production, the electron-donating substrate for NADPH oxidase (13, 44). The fact that EOMA expresses only nox-4 implicates this isoform of gp91 as part of the pathology linked to hemangioendothelioma formation. This hypothesis is supported by results of this study, demonstrating that knockdown of nox-4 expression in EOMA cells attenuates the formation of hemangioendothelioma *in vivo*. This observation also is supported by recently published independent concurrent work in nude mice, demonstrating that a nox-4 inhibitor, fulvene-5, blocks growth of endothelial tumors in mice (6). Our results are based on data from immunocompetent mice that uniquely address additional key issues such as

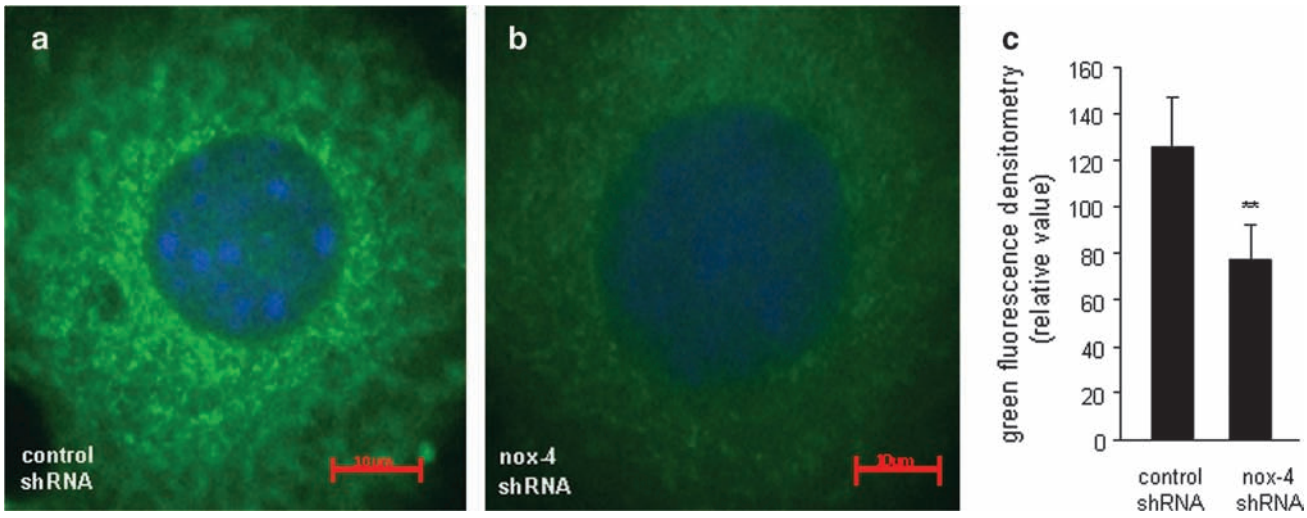

FIG. 8. Nox-4 is localized in the nuclear membrane region of EOMA cells. (**a**) Control shRNA or (**b**) nox-4 shRNA. (**c**) Quantitative comparison of perinuclear green fluorescence intensity was done by using Zeiss AxioVision software. Analysis was performed on three cells transduced with control shRNA and compared with results from three cells transduced with nox-4 shRNA. Loss of signal in knockdown cells confirms the specificity of the antibody used for nox-4. $^{**}p < 0.01$. (For interpretation of the references to color in this figure legend, the reader is referred to the web version of this article at www.liebertonline.com/ars).

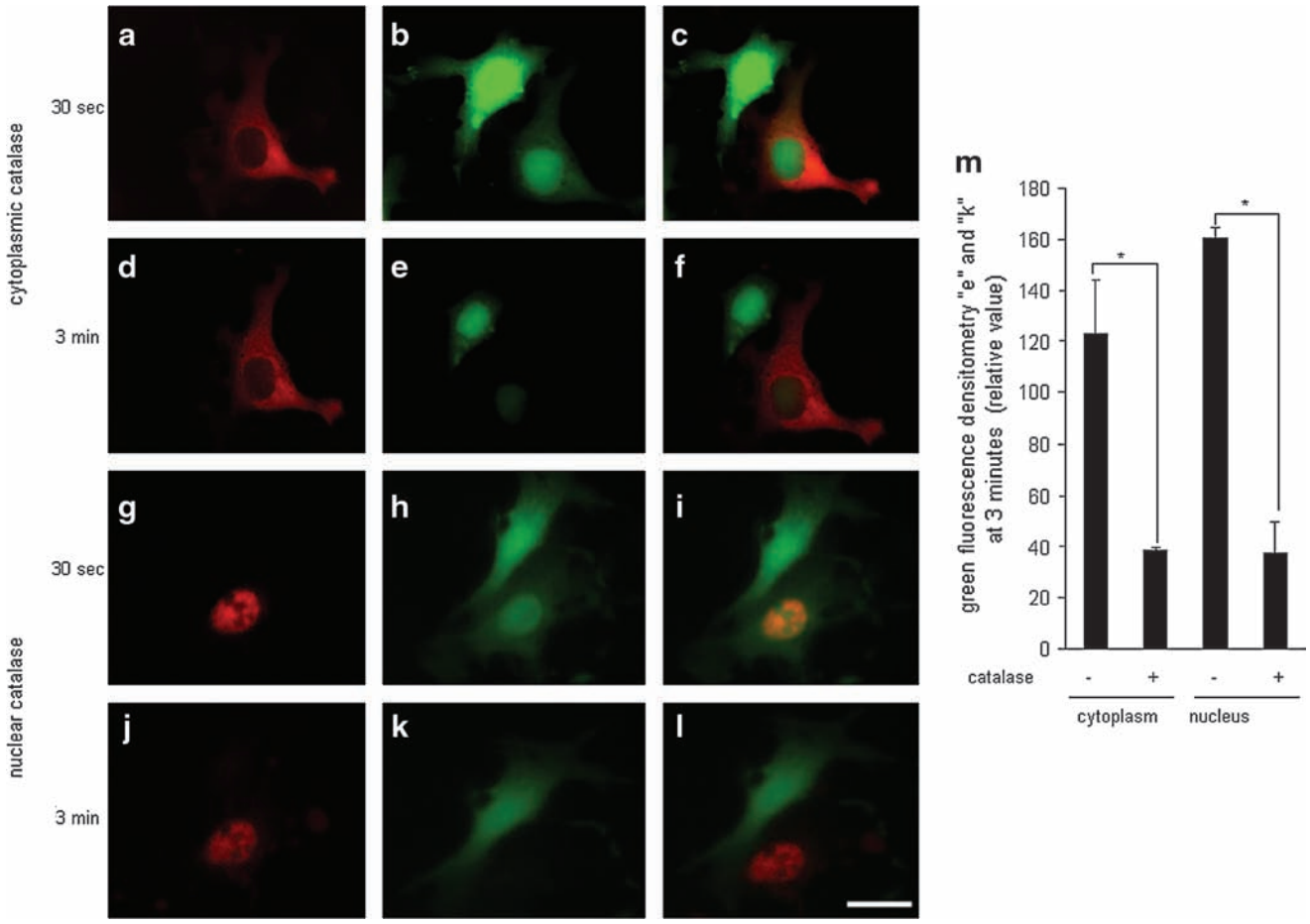

FIG. 9. Nox-4 delivers H_2O_2 directly into the nucleus of EOMA cells. Catalase (0.1 mU/cell) tagged with Qdot was microinjected to the cytoplasm [(**a**) catalase; (**b**) DCF; (**c**) merged image 30 s after injection; (**d**) catalase; (**e**) DCF; (**f**) merged image 3 min after injection) or the nucleus of an EOMA cell (**g**) catalase; (**h**) DCF; (**i**) merged image 30 s after injection; (**j**) catalase; (**k**) DCF; (**l**) merged image 3 min after injection]. Three minutes after microinjection, catalase-injected cytoplasm (**e**) and nucleus (**k**) showed lower DCF intensity (**m**). Results are expressed as mean ± SD. $*p < 0.05$; *white scale bar*, lower right hand corner = 30 μm. Catalase-sensitive DCF signal in the nucleus confirms that the DCF oxidation signal noted was generated by H_2O_2. (For interpretation of the references to color in this figure legend, the reader is referred to the web version of this article at www.liebertonline.com/ars).

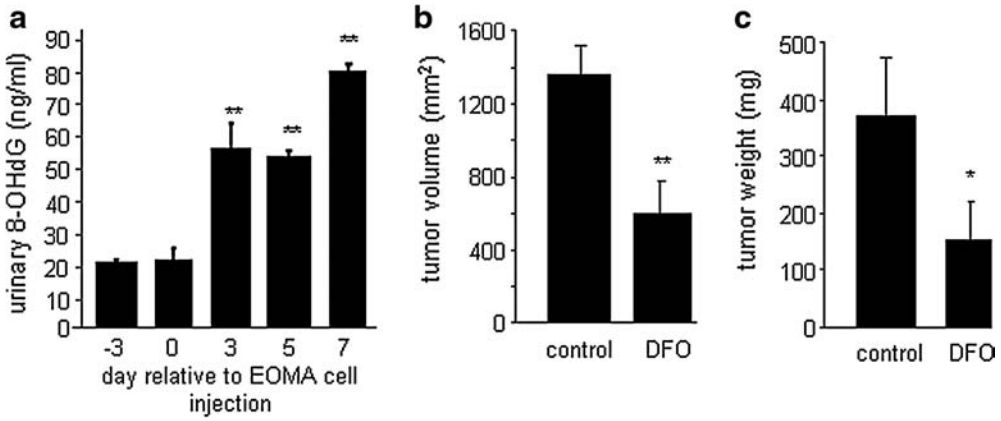

FIG. 10. Urinary excretion of oxidatively modified DNA from tumor-bearing mice and the effect of treatment with iron chelator DFO. (**a**) Pooled urine samples were collected on specified days from mice injected with EOMA cells. 8-Hydroxy-2′-deoxyguanosine (8-OHdG) was detected in the urine. No difference in 8-OHdG levels at day –3 and day 0, but days 3, 5, and 7 all had significantly elevated levels compared with baseline/day 0 values ($**p < 0.01$, ANOVA). To determine whether ferrous iron contributed to oxidative modification of DNA, tumor-bearing mice were treated with deferoxamine (DFO), an FDA-approved drug that functions as an iron chelator. Mice received daily intraperitoneal (IP) injection of either 0.1 ml of PBS (vehicle control) or DFO (100 mg/kg) beginning at day –1 relative to EOMA cell injection. KHE samples were collected at 7 days after EOMA cell injection, and calipers were used to measure (**b**) volume (length×width×height) and (**c**) mass. Mice treated with DFO had significantly smaller KHE for both volume and weight. $**p < 0.01$.

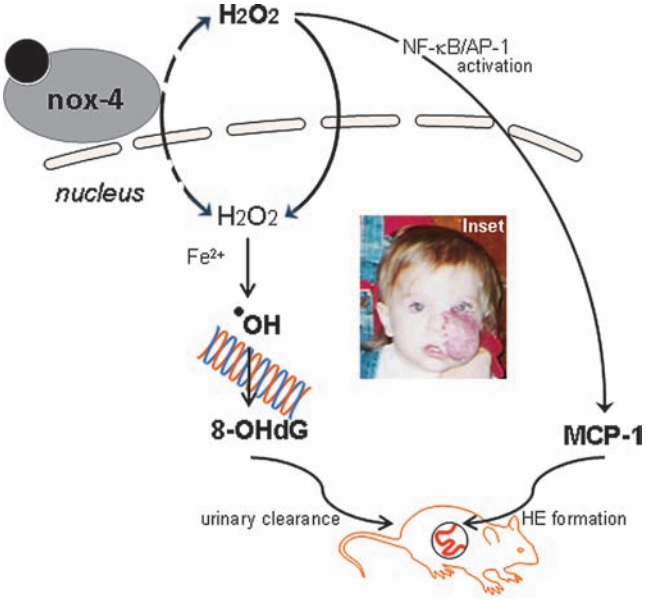

FIG. 11. The Nox-4-MCP1 axis of control for hemangioendothelioma formation. Nox-4–derived hydrogen peroxide drives MCP-1 expression, which was previously shown to be a key driver of HE formation. Nox-4–derived nuclear hydrogen peroxide, through an Fe^{2+}-dependent mechanism, causes oxidative modification of DNA, forming 8-OHdG. 8-OHdG clears through the urine of tumor-bearing mice and may be considered a biomarker candidate. **Inset:** Appearance of hemangioma or hemangioendothelioma tumor in children (informed consent obtained). (For interpretation of the references to color in this figure legend, the reader is referred to the web version of this article at www.liebertonline.com/ars).

the nuclear redox compartment, which in turn leads to the recognition of a potential urinary biomarker. Furthermore, taken together with our previous work on this project, the current work recognizes a key interplay between nox-4 and MCP-1 in driving the formation of hemangioendothelioma *in vivo* (20). MCP-1 is a particularly important target because it has been linked to poor clinical outcomes in humans for many other solid tumors (24, 29, 41, 43, 45, 48). In this work, we report that knockdown of nox-4 in EOMA cells inhibits MCP-1 expression markedly.

Current studies in redox signaling underscore the key issue of redox compartmentalization (23, 33, 39, 49). This addresses the issue of how freely diffusible ROS can activate redox signaling. Subcellular distribution of NADPH oxidases has an important bearing on intracellular redox compartments (49). This work presents the first evidence demonstrating that in EOMA cells, nox-4 derived ROS floods the nuclear compartment. The primary form of ROS derived from nox-4 is H_2O_2. Microinjection of catalase into subcellular compartments was instrumental in recognizing the DCF oxidation signal as being H_2O_2. The implications of these results are substantial, because oxidant loading in the nucleus makes nuclear DNA susceptible to oxidative modification. The significance of our nox-4–dependent nuclear H_2O_2 loading observation was substantially enhanced when we were able to detect oxidatively modified DNA In the urine of mice with hemangioendothelioma. The 8-OHdG levels are known to be elevated in the urine of humans with different types of cancers (50). These observations lead to the hypothesis that the observed nox-4–dependent nuclear oxidant loading is directly implicated in neoplastic transformation. Such a hypothesis is supported by our observation that iron chelation by DFO attenuates the size of hemangioendothelioma *in vivo*. It is well known that H_2O_2 alone may not be sufficient to trigger oxidative DNA damage. In the presence of ferrous iron, H_2O_2 may generate hydroxyl radical, which in turn may cause oxidative DNA damage, resulting in 8-OHdG formation and excretion (46).

In sum, the current state of information connects nox-4 to MCP-1 to form a major axis of control that regulates the fate of hemangioendothelioma development *in vivo* (see Fig. 11). This axis of control drives three interrelated processes: inflammation, angiogenesis, and cancer. Many examples exist of cancers arising in the setting of chronic inflammation, such as squamous cell carcinomas arising in chronic wounds. The converse observation that inflammation is present in cancers without an underlying chronic inflammatory condition also is true. The vast literature on the role of antiinflammatory cycloxygenase-2 inhibitors in suppressing the growth of colon, rectal, gastric, prostate, breast, thyroid, and skin cancers provides clear support for this concept. The overlap between inflammation and neoplastic transformation may be attributable to the fact that the same molecular events that trigger inflammation also trigger angiogenesis, which is required for the tumor to survive and propagate (11, 36). Thus, tumor-forming cells co-opt these pathways as part of the malignant transformation process. The nox4–MCP-1 axis is at the nexus of these pathways and represents high-value targets for the design of therapeutic strategies.

Acknowledgments

Funding for this work is supported by the NIH/NIGMS K08GM066964 (G.M.G.) and in part by NIH/NIDDK R01 DK076566 (S.R.).

Author Disclosure Statement

No competing financial interests exist.

References

1. Alom-Ruiz SP, Anilkumar N, and Shah AM. Reactive oxygen species and endothelial activation. *Antioxid Redox Signal* 10: 1089–1100, 2008.
2. Atalay M, Gordillo G, Roy S, Rovin B, Bagchi D, Bagchi M, and Sen CK. Anti-angiogenic property of edible berry in a model of hemangioma. *FEBS Lett* 544: 252–257, 2003.
3. Babior BM. The NADPH oxidase of endothelial cells. *IUBMB Life* 50: 267–269, 2000.
4. Bao JX, Jin S, Zhang F, Wang ZC, Li NJ, and Li PL. Activation of membrane NADPH oxidase associated with lysosome-targeted acid sphingomyelinase in coronary endothelial cells. *Antioxid Redox Signal* 12: 703–712, 2010.
5. Bedard K and Krause KH. The NOX family of ROS-generating NADPH oxidases: physiology and pathophysiology. *Physiol Rev* 87: 245–313, 2007.
6. Bhandarkar SS, Jaconi M, Fried LE, Bonner MY, Lefkove B, Govindajaran B, Perry BN, Parhar R, Mackelfresh J, Sohn A, Stouffs M, Knaus U, Yancopoulos G, Reiss Y, Benest AV, Augustin HG, and Arbiser JL. Fulvene-5 potently inhibits

NADPH oxidase 4 and blocks the growth of endothelial cell tumors in mice. *J Clin Invest* 119: 6, 2009.
7. Bokoch GM, Diebold B, Kim JS, and Gianni D. Emerging evidence for the importance of phosphorylation in the regulation of NADPH oxidases. *Antioxid Redox Signal* 11: 2429–2441, 2009.
8. Boye E, Yu Y, Paranya G, Mulliken JB, Olsen BR, and Bischoff J. Clonality and altered behavior of endothelial cells from hemangiomas. *J Clin Invest* 107: 745–752, 2001.
9. Burdon RH. Superoxide and hydrogen peroxide in relation to mammalian cell proliferation. *Free Radic Biol Med* 18: 775–794, 1995.
10. Condeelis J and Pollard JW. Macrophages: obligate partners for tumor cell migration, invasion, and metastasis. *Cell* 124: 263–266, 2006.
11. Costa C, Incio J, and Soares R. Angiogenesis and chronic inflammation: cause or consequence? *Angiogenesis* 10: 149–166, 2007.
12. Cristovao AC, Choi D, Baltazar G, Beal F, and Kim YS. The role of NADPH oxidase 1-derived reactive oxygen species in paraquat-mediated dopaminergic cell death. *Antioxid Redox Signal* 11: 2105–2118, 2009.
13. DeBerardinis RJ, Lum JJ, Hatzivassiliou G, and Thompson CB. The biology of cancer: metabolic reprogramming fuels cell growth and proliferation. *Cell Metab* 7: 11–20, 2008.
14. Dikalov SI, Dikalova AE, Bikineyeva AT, Schmidt HH, Harrison DG, and Griendling KK. Distinct roles of Nox1 and Nox4 in basal and angiotensin II-stimulated superoxide and hydrogen peroxide production. *Free Radic Biol Med* 45: 1340–1351, 2008.
15. Fischer H. Mechanisms and function of DUOX in epithelia of the lung. *Antioxid Redox Signal* 11: 2453–2465, 2009.
16. Folkman J, Mulliken J, and Ezekowitz R. Angiogenesis and hemangiomas. In: *Surgery of Infants and Children: Scientific Principles and Practice,* edited by Oldham K. Philadelphia: Lippincott-Raven, 1997, pp. 569–584.
17. Frey RS, Ushio-Fukai M, and Malik A. NADPH oxidase-dependent signaling in endothelial cells: role in physiology and pathophysiology. *Antioxid Redox Signal* 11: 791–810, 2009.
18. Frey RS, Ushio-Fukai M, and Malik AB. NADPH oxidase-dependent signaling in endothelial cells: role in physiology and pathophysiology. *Antioxid Redox Signal* 11: 19, 2009.
19. Gordillo G, Fang H, Khanna S, Harper J, Phillips G, and Sen C. Oral administration of blueberry inhibits angiogenic tumor growth and enhances survival of mice with endothelail cell neoplasm *Antioxid Redox Signal* 11: 47–58, 2009.
20. Gordillo G, Onat D, Stockinger M, Roy S, Atalay M, Beck M, and Sen C. A key angiogenic role of monocyte chemoattractant protein-1 in hemangioendothelioma proliferation. *Am J Physiol (Cell)* 287: C866–C873, 2004.
21. Gordillo GM, Atalay M, Roy S, and Sen CK. Hemangioma model for in vivo angiogenesis: inducible oxidative stress and MCP-1 expression in EOMA cells. *Methods Enzymol* 352: 422–432, 2002.
22. Griffith B, Pendyala S, Hecker L, Lee PJ, Natarajan V, and Thannickal VJ. NOX enzymes and pulmonary disease. *Antioxid Redox Signal* 11: 2505–2516, 2009.
23. Guzik TJ and Griendling KK. NADPH oxidases: molecular understanding finally reaching the clinical level? *Antioxid Redox Signal* 11: 2365–2370, 2009.
24. Hefler L, Tempfer C, Heinze G, Mayerhofer K, Breitenecker G, Leodolter S, Reinthaller A, and Kainz C. Monocyte chemoattractant protein-1 serum levels in ovarian cancer patients. *Br J Cancer* 81: 855–859, 1999.
25. Isik F, Rand R, Gruss J, Benjamin D, and Alpers C. Monocyte chemoattractant protein-1 mRNA expression in hemangiomas and vascular malformations. *J Surg Res* 61: 71–76, 1996.
26. Krishan A. Rapid flow cytofluorometric analysis of mammalian cell cycle by propidium iodide staining. *J Cell Biol* 66: 188–193, 1975.
27. Lambeth JD, Kawahara T, and Diebold B. Regulation of Nox and Duox enzymatic activity and expression. *Free Radic Biol Med* 43: 319–331, 2007.
28. Laurindo FR, Fernandes DC, and Santos CX. Assessment of superoxide production and NADPH oxidase activity by HPLC analysis of dihydroethidium oxidation products. *Methods Enzymol* 441: 237–260, 2008.
29. Leek RD, Lewis CE, Whitehouse R, Greenall M, Clarke J, and Harris AL. Association of macrophage infiltration with angiogenesis and prognosis in invasive breast carcinoma. *Cancer Res* 56: 4625–4629, 1996.
30. Leto TL, Morand S, Hurt D, and Ueyama T. Targeting and regulation of reactive oxygen species generation by Nox family NADPH oxidases. *Antioxid Redox Signal* 11: 2607–2619, 2009.
31. Lin EY, Nguyen AV, Russell RG, and Pollard JW. Colony-stimulating factor 1 promotes progression of mammary tumors to malignancy. *J Exp Med* 193: 727–740, 2001.
32. Lu Y, Chen Q, Corey E, Xie W, Fan J, Mizokami A, and Zhang J. Activation of MCP-1/CCR2 axis promotes prostate cancer growth in bone. *Clin Exp Metastasis* 26: 161–169, 2009.
33. Mofarrahi M, Brandes RP, Gorlach A, Hanze J, Terada LS, Quinn MT, Mayaki D, Petrof B, and Hussain SN. Regulation of proliferation of skeletal muscle precursor cells by NADPH oxidase. *Antioxid Redox Signal* 10: 559–574, 2008.
34. Nistala R, Whaley-Connell A, and Sowers JR. Redox control of renal function and hypertension. *Antioxid Redox Signal* 10: 2047–2089, 2008.
35. O'Reilly M, Brem H, and Folkman J. Treatment of murine hemangioendotheliomas with the angiogenesis inhibitor AGM-1470. *J Pediatr Surg* 30: 325–330, 1995.
36. Ono M, Torisu H, Jun-ichi F, Nishie A, and Michihiko K. Biological implications of macrophage infiltration in human tumor angiogenesis. *Cancer Chemother Pharmacol* 43: S69–S71, 1999.
37. Paller AS. Responses to anti-angiogenic therapies. *J Invest Dermatol Symp Proc* 5: 83–86, 2000.
38. Peshavariya HM, Dusting GJ, and Selemidis S. Analysis of dihydroethidium fluorescence for the detection of intracellular and extracellular superoxide produced by NADPH oxidase. *Free Radic Res* 41: 699–712, 2007.
39. Petry A, Djordjevic T, Weitnauer M, Kietzmann T, Hess J, and Gorlach A. NOX2 and NOX4 mediate proliferative response in endothelial cells. *Antioxid Redox Signal* 8: 1473–1484, 2006.
40. Pollard JW. Tumour-educated macrophages promote tumour progression and metastasis. *Nat Rev Cancer* 4: 71–78, 2004.
41. Saji H, Koike M, Yamori T, Saji S, Seiki M, Matsushima K, and Toi M. Significant correlation of monocyte chemoattractant protein-1 expression with neovascularization and progression of breast carcinoma. *Cancer* 92: 1085–1091, 2001.
42. Sorce S and Krause KH. NOX enzymes in the central nervous system: from signaling to disease. *Antioxid Redox Signal* 11: 2481–2504, 2009.
43. Tanaka K, Kurebayashi J, Sohda M, Nomura T, Prabhakar U, Yan L, and Sonoo H. The expression of monocyte chemotactic protein-1 in papillary thyroid carcinoma is correlated

with lymph node metastasis and tumor recurrence. *Thyroid* 19: 21–25, 2009.
44. Thompson CB. Metabolic enzymes as oncogenes or tumor suppressors. *N Engl J Med* 360: 813–815, 2009.
45. Torisu H, Ono M, Kiryu H, Furue M, Ohmoto Y, Nakayama J, Nishioka Y, Sone S, and Kuwano M. Macrophage infiltration correlates with tumor stage and angiogenesis in human malignant melanoma: possible involvement of TNFalpha and IL-1alpha. *Int J Cancer* 85: 182–188, 2000.
46. Toyokuni S and Sagripanti JL. Iron chelators modulate the production of DNA strand breaks and 8-hydroxy-2′-deoxyguanosine. *Free Radic Res* 31: 123–128, 1999.
47. Turchan-Cholewo J, Dimayuga VM, Gupta S, Gorospe RM, Keller JN, and Bruce-Keller AJ. NADPH oxidase drives cytokine and neurotoxin release from microglia and macrophages in response to HIV-Tat. *Antioxid Redox Signal* 11: 193–204, 2009.
48. Ueno T, Toi M, Saji H, Muta M, Bando H, Kuroi K, Koike M, Inadera H, and Matsushima K. Significance of macrophage chemoattractant protein-1 in macrophage recruitment, angiogenesis, and survival in human breast cancer. *Clin Cancer Res* 6: 3282–3289, 2000.
49. Ushio-Fukai M. Compartmentalization of redox signaling through NADPH oxidase-derived ROS. *Antioxid Redox Signal* 11: 1289–1299, 2009.
50. Valavanidis A, Vlachogianni T, and Fiotakis C. 8-Hydroxy-2′-deoxyguanosine (8-OHdG): a critical biomarker of oxidative stress and carcinogenesis. *J Environ Sci Health Part C* 27: 19, 2009.

Address correspondence to:
Gayle Gordillo, M.D.
915 Olentangy River Road, Suite 2100
Columbus, OH 43212

E-mail: gayle.gordillo@osumc.edu

Date of first submission to ARS Central, September 24, 2009; date of final revised submission, October 9, 2009; date of acceptance, October 9, 2009.

Abbreviations Used

AP-1 = activator protein-1
BrdU = bromodeoxyuridine
DCF = 5-(and-6)-carboxy-2′,7′ dichlorofluorescein diacetate
DFO = deferoxamine
DHE = dihydroethidium
EC = endothelial cell
HIF-1α = hypoxia-inducible factor-1 alpha
H_2O_2 = hydrogen peroxide
IP = intraperitoneal
IU = international unit
KHE = kaposiform hemangioendothelioma
MAE = murine aortic endothelial cell
MCP-1 = monocyte chemoattractant protein-1
NADPH oxidase = nicotinamide adenine dinucleotide phosphate oxidase
NF-κB = nuclear factor-kappa B
NGM = normal growth medium
8-OHdG = 8-hydroxy-2 deoxyguanosine
shRNA = short hairpin RNA
siRNA = small interfering RNA
VEGF = vascular endothelial growth factor